ON THE NEAR-FIELD FLOW STRUCTURE, TURBULENCE AND RESULTING CAVITATION IN JETS

Shridhar Gopalan
Department of Mechanical Engineering, The Johns Hopkins University
Baltimore, MD 21218, USA

Joseph Katz
Department of Mechanical Engineering, The Johns Hopkins University
Baltimore, MD 21218, USA

Omar Knio
Department of Mechanical Engineering, The Johns Hopkins University
Baltimore, MD 21218, USA

ABSTRACT

Cavitation experiments performed in the near field of a 50-mm diameter (D) jet at $Re_D=5x10^5$, showed inception in the form of inclined "cylindrical" bubbles at axial distances (x/D) less than 0.55, with indices of 2.5. On tripping the boundary layer, cavitation inception occurred at x/D ≈ 2, as distorted "spherical" bubbles with inception indices of 1.7. The cavitation event rates were measured using a piezoelectric pressure transducer. To investigate these substantial differences, the near field of the jet was measured using PIV. Three types of PIV measurements were performed in the near field - (a) 2-D velocity, vorticity and strain in the shear layer at specific phases. 50-60 such realizations were obtained for each of the two cases. Phase averaged velocity, vorticity, strain rate and Reynolds stresses were then calculated. (b) High magnification (~4) images of the separating boundary layer (at x/D ~ 0.007) were obtained to measure the velocity profile (i.e. inlet boundary conditions). Momentum thickness (Θ), displacement thickness (δ*) were then estimated for the two cases. (c) The velocity field in planes parallel to the jet axis but offset from the center at two locations: rcosΦ=0.53D and 0.55D (Φ is the azimuthal angle measured from the horizontal) were also obtained. This plane gives data on the "streamwise" vortices. The untripped case showed a direct transition to three-dimensional flow dominated by strong "streamwise" vortices with strengths up to 25% of the jet velocity times the characteristic wavelength. Cavitation inception occurred in these vortices. Prominent vortex rings were only seen beyond x/D≈0.7. In contrast in the tripped jet the vortex sheet rolled up to familiar Kelvin-Helmholtz vortex rings with weaker "streamwise" vortices. Also the Reynolds stresses in the near field of the jet show similar trends and magnitudes to those of Browand & Latigo (1979) and Bell & Mehta (1990) for a plane shear layer.

INTRODUCTION

This paper deals with the near-field flow structure in circular jets at high Reynolds numbers and the associated cavitation. To examine the effect of Θ/D (i.e. to see the effect of changing the characteristics of the initial boundary layer) on cavitation, experiments were performed with and without boundary layer tripping. It was observed that, for the untripped (or smooth) jet, cavitation inception occurred in the near field (x/D < 0.6) as "cylindrical bubbles", in what appeared to be secondary riblets. However, in the tripped jet cavitation inception appeared at x/D~2 in primary vortices, as distorted, more or less "spherical" bubbles. The "cylindrical" bubbles observed in the smooth jet suggest that "secondary" structures play a more important role in the smooth jet than in the tripped jet. In order to investigate the causes for such substantial differences on tripping the boundary layer, the focus of this research shifted to the near-field flow structure, with and without boundary layer tripping. Consequently, PIV was used to measure the shear layer of the jet in the region x/D<1. In Gopalan *et al.* (1998a, b, c) & Gopalan (1998) data on the bubble distributions, photographs of cavitating bubbles during inception, cavitation inception measurements, shear layer (primary flow) measurements and strain rate distributions are presented in detail. This paper focuses on Reynolds stresses in the near field, the secondary flow and separating boundary layer measurements and elucidates the differences between the untripped and tripped jets. Using the PIV data, the cavitation event rates were estimated and compared to the measured event rates (Gopalan 1998, Gopalan *et al.* 1998c).

EXPERIMENTAL APPARATUS

The experiments were performed in a specially designed closed-loop jet cavitation facility located at Johns Hopkins University. The main test chamber is 1.98 m long and its

cross-section is 0.69 x 0.76 m^2. It has windows on four sides to enable easy access for PIV and holographic measurements. The flow is driven by two 15 HP centrifugal pumps located about 4 m below the nozzle in order to prevent pump cavitation. In this study the jet velocity was fixed at 10 m/s (Re_D = 5x10^5) and the cavitation index was varied by varying the pressure in the test chamber. The air content was reduced to about 3 ppm by keeping the facility under vacuum for extended periods and the dissolved oxygen content determined using an oxygen meter. Glass injectors installed inside honeycombs supplied the bubbles (nuclei) for cavitation. The 50.8-mm diameter jet was injected from a smooth, 2:1 diameter ratio cosine shaped circular nozzle. The length of the nozzle is 76.2 mm. For experiments with a tripped boundary layer an extension tube was attached at the exit of the original nozzle as shown in figure 1. This extension has 16 circumferential, axisymmetric trips (i.e. ring-like protrusions) of height 0.5 mm in a 6.35mm region and the remaining 19mm wall is smooth. Figure 2 shows the region where PIV data and phase-averaged bubble distributions were recorded. A piezo-electric pressure transducer (PCB 102A05) with a resonance frequency of 300 kHz, located close to but outside of the jet sensed the motion of large-scale vortices and was used to record data at specific phases (i.e. conditional sampling of data). Typically, data were recorded either at the positive peak (between two eddies) or the negative peak (an eddy near by) of the pressure signal (figure 2). The transducer was also used for detecting the occurrence of cavitation. Velocity measurements were performed using PIV, following procedures detailed in (Dong *et al.* 1992, Roth *et al.* 1995, Sridhar & Katz 1995). Detailed background on PIV can be found in (Adrian 1991). This method consists of recording multiple (in this case, double) exposure images of particle tracers in a flow field illuminated by a pulsed laser sheet. The displacement of the particle during the known time interval then gives the local velocity. The laser used was a two head frequency doubled Nd:YAG laser (wavelength=532nm), capable of pulse energies up to 300mJ.The camera used were a 2K × 2K pixel^2 camera with hardware-based image shifting and a film camera with electrooptic image shifting. Particles used were 20-45μm fluorescent and 5-12μm silver-coated glass spheres.

MEASUREMENTS OF THE SEPARATING BOUNDARY LAYER

To complete the picture of the near field flow, one needs the characteristics of the separating boundary layer. The rest of the parameters including the jet diameter, the Reynolds number, Strouhal number (St_D~1.0 at x/D=0.375) and wavelength λ=0.25D (both for the untripped jet) are known. In this section we provide data on the initial momentum thickness, Θ and the shape factor for the untripped and tripped boundary layers. High magnification PIV with a field of view of 6.3mm was used to record data. The vector spacing was 200μm. Table 1 shows the displacement thickness (δ^*), momentum thickness (Θ) and the shape factor δ^*/Θ calculated from the velocity profiles at x/D=0.0073 for the untripped and x/D=0.0071 for the tripped jet respectively. The results are compared to classical data taken

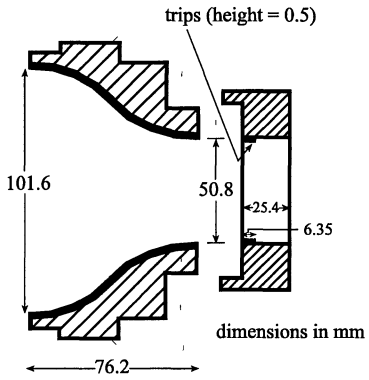

Figure 1. Dimensions of the nozzle and the extension with trips.

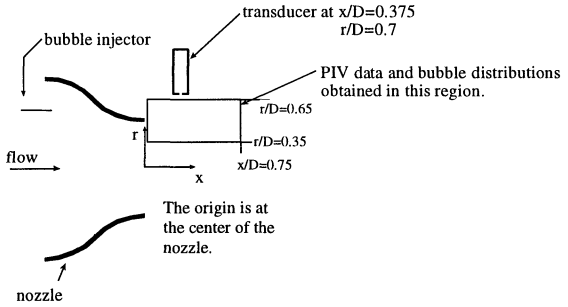

Figure 2. Close-up of region where data on the primary flow was obtained.

TABLE 1	δ^* μm	Θ (μm)	Shape factor δ^*/Θ
Smooth jet	393	110	3.4
Tripped jet	417	201	2.07
(I)	-	-	2.6
(II)	-	-	1.3
(III)	-	107 - 351	2.37 - 2.6
(IV)	-	262 - 483	1.51 - 1.6

from Burmeister 1993 for a flat plate with laminar (I) and turbulent boundary layers (II) and to those of Hussain & Zedan (1978) for a circular jet with laminar (III) and turbulent boundary layers (IV). The drop in the shape factor of the boundary layer from 3.4 to 2.07 on tripping it is consistent with a turbulent boundary layer after it transitions from laminar. For a flat plate shape factors ranging from 2.55-1.4 correspond to the region of transition.

UNTRIPPED JET (PRIMARY FLOW)

As will be demonstrated using other interrogation planes (the section on "secondary" vortices), the existence of vorticity peaks at r/D ≥ 0.53D x/D<0.5, in figure 3a, is associated with the flow becoming three-dimensional immediately after exiting from the nozzle, even before rolling up to distinct vortex rings. Prominent vortex rings are

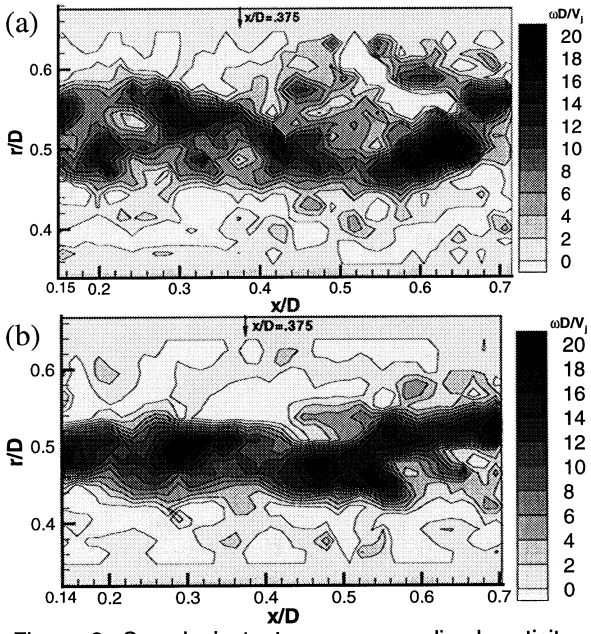

Figure 3. Sample instantaneous normalized vorticity for (a) smooth (b) tripped jet during a positive pressure peak at x/D=0.375.

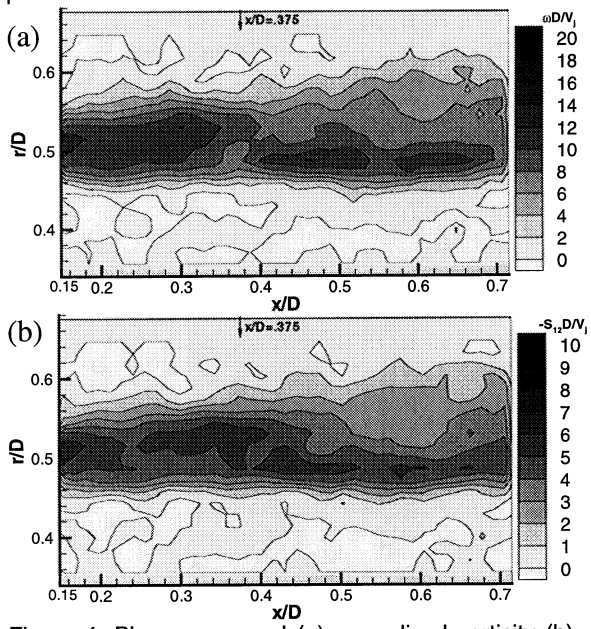

Figure 4. Phase averaged (a) normalized vorticity (b) normalized strain in the smooth jet for data recorded at a positive pressure peak at x/D=0.375.

observed beyond x/D=0.7. In the domain x/D < 0.5, the thin, laminar boundary layer separating from the nozzle, is highly unstable and portions of this vortex sheet are locally displaced into the external slow moving fluid. These portions are rapidly stretched by the steep velocity gradient, resulting in the formation of strong "streamwise" vortices along the principal strain axis. In some cases these structures resemble hairpin vortices, which was noted from counter rotating vorticity pairs in measurements described in the section on "secondary" vortices. This near field behavior of the smooth jet is very different from roll up to vortex rings typically seen in shear layers, including the present tripped jet. Confirming the results of the bubble distributions (Gopalan 1998), there is also a characteristic wavelength λ = 0.25D-0.3D, that is sensed by the trigger transducer.

TRIPPED JET (PRIMARY FLOW)

The vorticity distribution in figure 3b shows prominent spanwise structures (rings) with peaks roughly aligned along r/D=0.5, quite consistent with a typical shear layer. The thinning vorticity region between the vortex rings coincides well with the location of the trigger transducer. In this sample map, one can also see vortex pairing at about x/D=0.6. Similar trends in vorticity and strain were seen in 57 instantaneous realizations. Thus, in the near field of the tripped jet, the thicker turbulent boundary layer rolls up to prominent Kelvin-Helmholtz vortex rings. In this case the wavelength λ=0.15D-0.2D. Note that the strength of the strain field in the tripped jet is similar to that of the smooth jet (the strain distributions for the two cases are presented in Gopalan et al., 1998c and figures 4&5). Thus, the magnitude of the strain rate (stretching "secondary" vortices) was clearly not the primary cause for the differences observed, in the conditions and appearance for cavitation inception. This

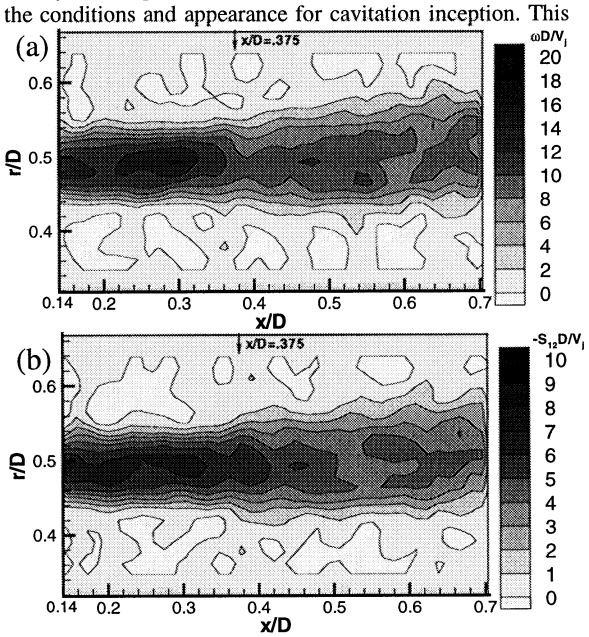

Figure 5. Phase averaged (a) normalized vorticity (b) normalized strain in the tripped jet for data recorded at a positive pressure peak at x/D=0.375.

indicates that the strengths of the "secondary" vortices where cavitation inception occurs must be much higher in the smooth jet than in the tripped jet (which is also evident from the discussions for the untripped jet). This conclusion led to velocity measurements in planes that provide data directly on the strength of these vortices.

Phase-averaged distributions of vorticity and strain rate are presented in figures 4 and 5. Phase averaging has smeared the features observed in the instantaneous plots, but one still can see that the shear layer of the smooth jet extends to a higher r/D compared to the tripped case. Also, in the smooth case (figure 4a) regions with high vorticity expand to higher radial locations whereas in the tripped jet (figure 5a) there is a clear peak at x/D=0.3, r/D≈0.5. It is evident that much of the difference between the smooth and tripped jets has been lost by phase averaging, indicating that our method of conditional sampling does not account for the variability caused by the "secondary structures".

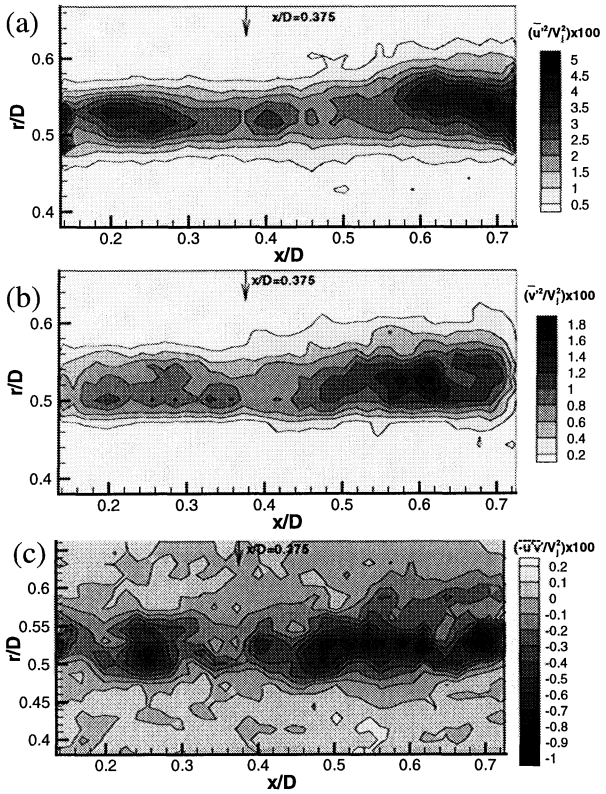

Figure 6. Distributions of (a) $\overline{u'^2}$ (b) $\overline{v'^2}$ (c) $-\overline{u'v'}$ in the smooth jet for data recorded at a positive pressure peak at x/D=0.375.

REYNOLDS STRESSES

Distribution of turbulence stresses $\overline{u'^2}, \overline{v'^2}$ and $-\overline{u'v'}$ are plotted for the smooth and tripped cases in figures 6 and 7, respectively. Here $u' = u - \bar{u}$ and $v' = v - \bar{v}$ where (u, v) is the instantaneous velocity and $(\bar{u}, \bar{v})$ is the phase-averaged velocity obtained from 50 and 57 instantaneous realizations for the tripped and smooth cases respectively. Several trends are evident from the results. First, magnitudes of $\overline{u'^2}, \overline{v'^2}$ and $-\overline{u'v'}$ are higher in the smooth jet and they extend to higher radial locations than the corresponding values for the tripped jet. Second, there is a low level of fluctuations at the position corresponding to the trigger transducer. Third, there is no clear relationship between the location and magnitudes of the phase-averaged strains and shear stresses. In some both are high and at the same location (tripped jet at x/D=0.3) but in others there are conflicting trends (smooth jet at x/D=0.25). Fourth, in the smooth jet the peaks of the stresses consistently are located at r/D>0.5, whereas in the tripped jet they are aligned with r/D=0.5. In the tripped jet, the peaks coincide with peaks in the phase-averaged vorticity, but there is no obvious relationship in the smooth jet. Still, turbulent peaks in the smooth jet exist within regions of high vorticity; this suggest that the primary source of turbulence involves fluctuations in the locations (and strength) of the

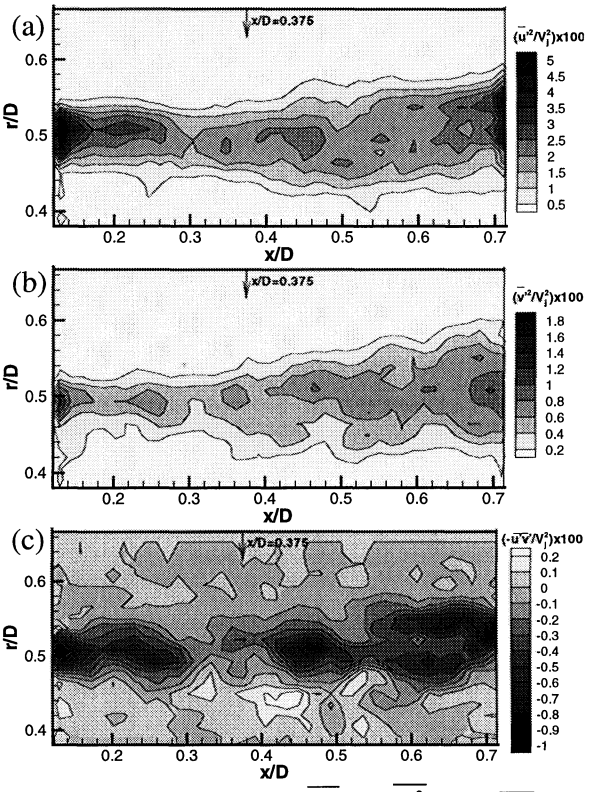

Figure 7. Distributions of (a) $\overline{u'^2}$ (b) $\overline{v'^2}$ (c) $-\overline{u'v'}$ in the tripped jet, for data recorded at a positive pressure peak at x/D=0.375.

vortex structures. The trends in the Reynolds stresses (especially maximum values in the untripped and tripped cases) are similar to measurements in a plane shear layer by Browand & Latigo (1979) and Bell & Mehta (1990). Browand & Latigo's data show that $\overline{u'^2}$ is higher in shear layers originating from a laminar boundary layer than in the turbulent case for x/Θ<800 and asymptotes to almost the same values downstream. This trend is also seen in our data. Their maximum normalized r.m.s magnitudes for the laminar case is 0.2 (at x/Θ~200), compared to 0.187 (at x/Θ~100 and 300) in our case. In the tripped case, their maximum value at 50 < x/Θ < 200 is about 0.14 which is the same in our case. This trend of the normal stresses in the very near field being higher in the untripped than in the tripped case is also

observed in Bell & Mehta measurements (1990) for a plane shear layer. Downstream the stresses asymptote to almost the same value, which cannot be seen in our case since our data extends up to x/D=0.72. Highest (normalized) magnitudes of $\overline{u'^2}$ in Bell & Mehta's results are 0.06 for the untripped case, compared to 0.035 in our case and about 0.03 (at x/Θ~175) for the tripped case, compared to 0.02 in our case. Normalized magnitudes of $\overline{v'^2}$ are much higher in their results, reaches values of 0.11 in the untripped case compared to 0.018 in our case. Nevertheless, the values of $\overline{v'^2}$ in the untripped case is about 4 to 6 times the value for the tripped case, which is comparable to a factor of 3 in our case. Normalized magnitudes of $-\overline{u'v'}$ are comparable in the untripped and tripped cases (for x/Θ< 320 or 175) and ranges from 0.007 to 0.014, similar to maximum values of 0.01 in our case.

MEASUREMENT OF VELOCITY FIELD IN PLANES THAT CUT THROUGH THE "SECONDARY" VORTICES

Data was recorded with the light sheet in planes parallel to the jet axis, at two positions rcosΦ=0.53D and 0.55D as shown in figure 8.

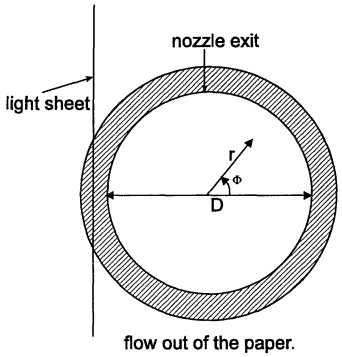

Figure 8. Orientation of the light sheet for capturing the "streamwise" vortices.

These planes cut through the inclined "streamwise" structures in the shear layer. Details of the procedure are presented in Gopalan (1998). Figure 9 shows sample instantaneous vorticity distribution for the smooth and the tripped cases. The distributions also show counter-rotating vortices spaced about 0.05D apart, which is one signature of a hairpin vortex (the other being the radially displaced vortex in the vorticity distributions in figure 3a). Thus we see the existence of intermittent hairpin like vortices in the near field. Also note that the vorticity map for the smooth jet (figure 9a) shows a larger number of vortical regions as compared to figure 9b for the tripped jet. At the plane rcosΦ=0.55D in both cases, there is very little vortical fluid up to 0.4D, which is consistent with the radial spread of vorticity in figure 3a. 42 images were analyzed at the plane rcosΦ=0.53D in both cases, to obtain a distribution of the strength of the "streamwise" vortices. Since we were primarily interested in the estimation of peak negative pressures (relevant to cavitation inception), the highest

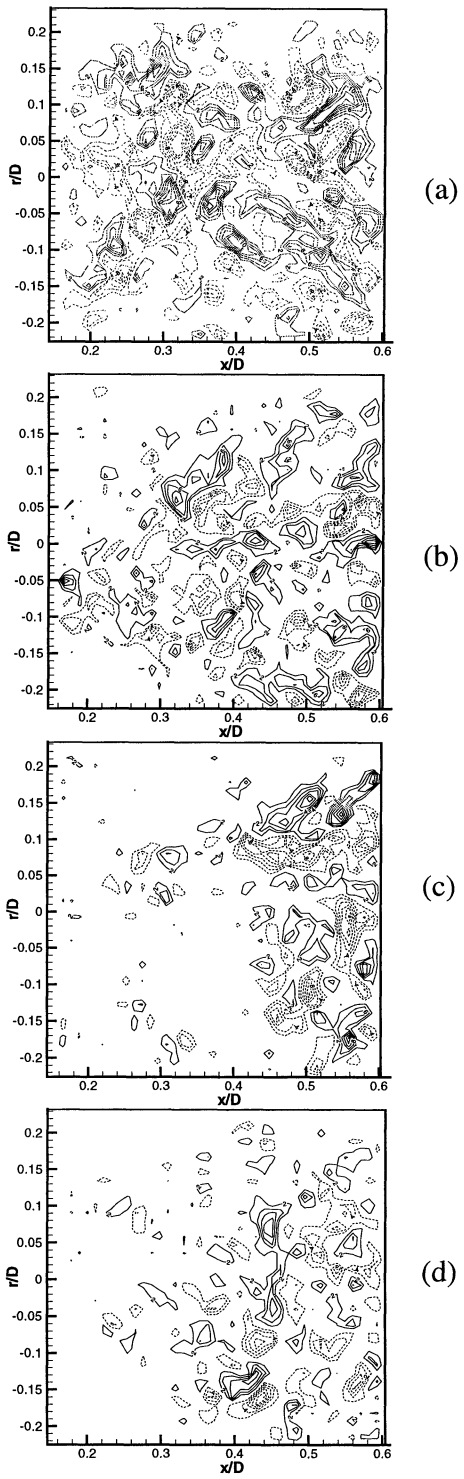

Figure 9. Instantaneous normalized vorticity ($\omega D/V_j$) distributions at rcosΦ=0.53D for (a) the smooth jet (b) tripped jet and at rcosΦ=0.55D for (c) smooth jet (d) tripped jet. Incremental lines represent a jump of 2 and dashed lines are negative vorticity. Zero is not shown.

circulation value chosen from every instantaneous map for both the smooth and tripped jets. The strength distributions are presented in figure 10. The abscissa for these plots is $\Gamma/V_j\lambda$, where λ=0.25D and $V_j\lambda$ is the total circulation within a wavelength. The distributions show that peaks for the smooth and the tripped nozzle occur at 16% and 2% of $V_j\lambda$ respectively. Strengths above 19% of $V_j\lambda$ occur 30% of the time for the smooth jet, and never for the tripped jet. Thus, the secondary" vortices in the smooth jet are substantially

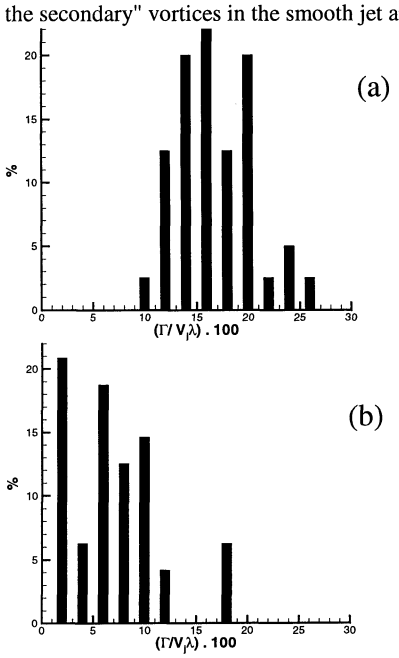

Figure 10. Distribution of highest strengths of "streamwise" vortices in the region 0.15D<x<0.6D for (a) smooth and (b) tripped jet.

stronger than those in the tripped jet. This striking result identifies the primary difference between the two cases. Bell & Mehta (1993) performed experiments with a plane shear layer at $Re_\delta = 2.9\times10^4$, with untripped and tripped boundary layers. They find the average streamwise circulation to be 10% of the spanwise circulation, for the untripped case. On tripping the boundary layer, they did not observe spatially stationary streamwise vortices. Thus, our trend of diminishing three-dimensionality on tripping the boundary layer is consistent with Bell & Mehta's data. However we differ significantly on (relative) magnitude. In summary, the results show that a "secondary" vortex in the very near field of the smooth jet can have up to a quarter of the circulation per wavelength, highlighting the strong three-dimensionality of the near field.

CONCLUSIONS

A 50-mm jet ($Re_D = 5\times10^5$) with an initially laminar boundary layer at $Re_\Theta = 1100$ ($\delta^*/\Theta = 3.4$), showed transition to three-dimensional flow in the very near field with strong "streamwise" vortical structures. The strengths of these vortices reached levels of 25% of $V_j\lambda$. Tripping the boundary layer increased Re_Θ to 2010 and reduced δ^*/Θ to values characteristic of a turbulent velocity profile. It also resulted in formation of the familiar Kelvin - Helmholtz vortex rings with significantly weaker secondary vortices. This change had a significant impact on the cavitation inception characteristics in the jet (Gopalan *et al.* 1998c).

ACKNOWLEDGMENTS

The jet project has been supported in early stages by Office of Naval Research (Program Manager- Dr. Ed Rood), under grant no. N00014-95-J-0329 and since 1997 by National Science Foundation (Program Manager- Prof. Roger Arndt), under grant no. CTS-9706701.

REFERENCES

Adrian, R. J., 1991 Particle-imaging techniques for experimental fluid mechanics *Ann. Rev. Fluid Mech.* **23**, 261.

Arndt, R. E. A. 1981 Cavitation in fluid machinery and hydraulic structures. *Ann. Rev. Fluid Mech.* **13**, 273-328.

Arndt, R.E.A. 1995 Vortex Cavitation in *Fluid Vortices*, S.I. Green (Ed.), Springer-Verlag; NY, pp.731-782.

Batchelor, G. K. 1967 *An Introduction to Fluid Dynamics*. Cambridge University Press.

Bell, J. H. & Mehta, R. D. 1990 Development of a two-stream mixing layer from tripped and untripped boundary layers. *AIAA journal*, **28**, 2034-2042.

Bell, J. H. & Mehta, R. D. 1993 Effects of imposed spanwise perturbations on plane mixing-layer structure. *J. Fluid Mech.* **257**, 33-63.

Burmeister, L. C. 1993 *Convective heat transfer,* John Wiley & Sons, Inc.

Dong, R., Chu, S., & Katz, J. 1992 Quantitative Visualization of The Flow Structure Within The Volute of a Centrifugal Pump, Part A: Technique, *J. Fluids Eng.*, 114, 390-395.11.

Gopalan, S., Katz, J., & Knio, O. 1998a The Near Field Flow Structure and its Effect on Cavitation Inception in Jets, 1998 ASME Fluids Engineering Division Summer Meeting, Washington D.C., June 1998.

Gopalan, S., Katz, J., & Knio, O. 1998b Effect of boundary layer tripping on the onset of cavitation in jets. Third International Symposium on Cavitation, Grenoble, France, April 1998.

Gopalan, S., Katz, J., & Knio, O. 1998c The flow structure in the near field of jets and its effect on cavitation inception, submitted to *J. Fluid Mech.*

Gopalan, S. 1998 Part A: The flow structure in the near field of jets and its effect on cavitation inception, Ph.D. thesis, Johns Hopkins.

Hussain, A. K. M. F. & Zedan, M. F. 1978 Effects of the initial condition on the axisymmetric free shear layer: effects of the initial momentum thickness. *Phys. Fluids* **21**, July, 1100-1112.

Roth, G., Hart, D. & Katz, J. 1995 Feasibility of using the L64720 video motion estimation processor (MEP) to increase efficiency of velocity map generation for PIV, *ASME/EALA Sixth International Symposium on Laser Anemometry*, Hilton Head S.C.

Sridhar, G. & Katz, J. 1995 Lift and drag forces on microscopic bubbles entrained by a vortex. *Phys. Fluids* **7**, 389–399.